DOI: 10.1002/ ((please add manuscript number))
Article type: Full paper

Melamine Hydroiodide Functionalized $MAPbI_3$ Perovskite with Enhanced Photovoltaic Performance and Stability in Ambient Atmosphere

Fu Yang, Muhammad Akmal Kamarudin,* Daisuke Hirotani, *Putao Zhang, Gaurav Kapil, Chi Huey Ng, Tingli Ma, and Shuzi Hayase**

F. Yang, Dr. M. A. Kamarudin, D. Hirotani, P. T Zhang, Dr. G. Kapil, Dr. C. H. Ng, Prof. Dr. T. L. Ma, Prof. Dr. S. Hayase

Graduate School of Life Science and Systems Engineering Institution Kyushu Institute of Technology

2-4 Hibikino Wakamatsu-ku, Kitakyushu 808-0196, Japan

E-mail: yang-fu@edu.life.kyutech.ac.jp; hayase@life.kyutech.ac.jp

Keywords: $MAPbI_3$; Perovskite solar cells; Stability; ambient atmosphere; Two-dimensional

Abstract

Despite the remarkable performance of organometallic halide perovskite solar cells (PSCs), their ultimate stability is still major issue to inhibit the commercialization of this eminent technology. Herein, melamine hydroiodide (MLAI) was added to function methyl ammonium ($CH3NH3^+$, MA^+) lead iodide perovskite for fabricating structured perovskite with enhanced photovoltaic performance and stability in the harsh ambient atmosphere (35 ^oC, 60-70% relative humidity). Nearly no new phase formed even incorporated 25 mol% MLAI induces the strain in the perovskite crystal structure. The MLAI structured perovskite film showed denser and smoother surface than the pristine $MAPbI_3$ perovskite. Planar PSCs based on 2 mol% MLAI functionalized perovskite showed 17.2% power conversion efficiency with nearly no hysteresis which is much higher than pristine $MAPbI_3$ PSCs. Most importantly, the solar cell devices based on 2 mol% MLAI

functionalized perovskite still retain over 90% of the initial performance after kept in ambient atmosphere for more than 560 h without encapsulation.

Introduction

Following pioneering work in 2012[1], power conversion efficiency (PCE) of metal-halide perovskite solar cells (PSCs) has increased from 3.8% to 23.3% within just a few years, gaining tremendous attention from all over the world.[2] However, the most researched perovskite materials, i. e. $MAPbI_3$ (MA^+, methyl ammounium) still exhibit poor stability in ambient atmosphere. [3] Therefore, most researchers are trying to avoid the influence of ambient atmosphere by utilizing nitrogen/argon-filled glovebox, which incur additional cost and thus limit the commercialization and mass level production of PSCs.[4] Because the instability of MA^+ under thermal, moisture and oxygen, irreversible decomposing of $MAPbI_3$ to PbI_2 occurs easily and this will affect the performance of PSCs.[5] Many efforts have been focused to enhance the stability of perovskite layer. Controlling the crystal growth by adjusting the antisolvent can increase the quality of the morphology in perovskite layer.[6] Doping the perovskite layer with other metals ions has also been shown to increase the stability.[7] In addition, modifying the electron or hole blocking layer also can increase the perovskite layers stability.[8] Recently, partial substitution of MA^+ in $MAPbI_3$ perovskite with a larger organic ammonium cation (i. e. Phenylethyl ammonium, Butyl ammonium) to obtain 2D/3D hetero structured perovskite can great increase the stability of perovskite layer as the larger organic group has a high stability toward the moisture.[9] However, large organic cations which interacting with the $[PbI_6]^{4-}$ octahedra through the ionic and hydrogen bonding can induce an obvious structural changes.[10] In addition, the large organic cations will act as insulating spacing layers between the conductive inorganic slabs, resulting to inhibit charge

transport between the neighboring inorganic layers, which makes the performance of 2D/3D PSCs worse than that of 3D perovskite.[11] Through adjusting the ligand of diammonium cations($^{+}NH_3$-R-NH_3^{+}), Cheng et al. showed that there is no new phase formed in the $MAPbI_3$ perovskite by incorporation <5 mol% EDA^{2+} ($^{+}NH_3$-CH_2CH_2-NH_3^{+}) as they provide hydrogen bonding to $[PbI6]^{4-}$ at both ends, which increased the perovskite layer stability without decreasing the performance of PSCs.[12] However, this effect of the 2D/3D perovskites is so far observed on the EDA^{2+} cation. Thus, it is greatly desirable to develop alternative approaches for enhancing the stability of perovskite without creating new perovskite phase.

Herein, we introduced melamine hydroiodide (MLAI) to replace MAI for the $MA_{1-x}MLA_xPbI_3$ (x= 0, 0.01, 0.02, 0.05, 0.10, 0.25) perovskite. The MALA has three amine groups that may provide hydrogen bonding to $[PbI_6]^{4-}$, which is the key distinction from the previous studies. Even when the 25 mol% MLAI was incorporated into the $MAPbI_3$ perovskite, there is nearly no new phase formed in the crystal structure. This means formation of 2D structures was specifically excluded by using MLAI (Scheme 1), which is the key point to avoid the solar cell efficiency losing. In addition, The $MA_{1-x}MLA_xPbI_3$ perovskite film showed denser and smoother surface than the pristine $MAPbI_3$ perovskite. Furthermore, 2 mol % MLAI incorporated planar perovskite solar cell showed a high efficiency of 17.2% which is much high than that of pristine $MAPbI_3$ (13.7%). All the process of PSCs was performed in robust humid ambient atmosphere (35^{o}C, 60-70% relative humidity). Moreover, the PCE was kept over 90 % after solar cells were kept in the ambient atmosphere for more than 560 hours without encapsulation.

Results and Discussion

The $MA_{1-x}MLA_xPbI_3$ (x= 0, 0.01, 0.02, 0.05, 0.10, 0.25) hetero perovskite films were fabricated by one-step spin-coating method using ethyl acetate as the antisolvent. Figure 1a shows the XRD patterns of 2D/3D $MA_{1-x}MLA_xPbI_3$ (x= 0, 0.01, 0.02, 0.05) perovskite films on glass substrates. All the films were prepared in 60-70% relative humidity (RH) ambient atmosphere. Strong signals located at 14.1^o , 28.4^o and 31.9^o of 2θ corresponding to planes of (110), (220) and (222). [13] The XRD patterns obtained in this experiment are in accordance with previous reports of $MAPbI_3$ perovskite (I4/mcm (140) space group). [14] Moreover, a slight diffraction peak at 12.7 ^{o} shown in the pristine $MAPbI_3$ perovskite film corresponding to the PbI_2. However, this peak of PbI_2 disappeared after incorporation of MLAI for the hetero perovskite. This result indicates that MLAI suppressed phase segregation of PbI_2 by effectively coordinating the position of Pb^{2+} in the perovskite. In addition, even when x=0.25 MLAI was incorporated into the perovskite, nearly no diffraction peak was observed from 5^o to 10^o of 2θ (Figure S1a), indicating that no new phase formed in the perovskite crystal structure. Figure 1b shows relative strain as a function of MLAI content. It has been reported that perovskite materials with higher strain is prone to degradation due to ion migration.[15] The relative strain was calculated by Williamson-Hall plot using a linear fitting. It is found that when x=0.02, the relative strain is lowest. Moreover, the diffraction peaks shift slightly to lower angles upon increasing MLAI concentration as shown in Figure S1b. This result indicates that incorporation of larger organic group of MLAI induced unit cell expansion in the perovskite. Looking at the (110) facet, the interplanar spacing increased gradually from 6.265 Å to 6.275 Å from x=0 to x=0.02 (Figure 1c). However, for x>0.2, the volume expansion remains constant which is similar to the precious report. [11]

The surface morphologies of annealed $MA_{1-x}MLA_xPbI_3$ (x= 0, 0.01, 0.02, 0.05) hetero perovskite films were studied by field emission scanning electron microcopy (FE-SEM), shown in Figure 2.

All the perovskite films were prepared in ambient atmosphere (35 ^{o}C, 60-70% RH). All the $MA_{1-x}MLA_xPbI_3$ perovskite films showed homogeneous surface. However, there are some cracks (marked by red circle) in the $MAPbI_3$ perovskite film (Figure 2a). The cracks which mainly caused by mechanical stress due to fast crystal growth rate of the perovskite film.[16] However, the cracks disappeared when MLAI was incorporated into the perovskite. In addition, the perovskite films exhibit better morphology with dense and pinhole-free perovskite surface. It was observed that increasing MLAI content decrease the grain size of the perovskite. The average grain size is 396 nm for $MAPbI_3$, 314 nm for $MA_{0.99}MLA_{0.01}PbI_3$, 268 nm for $MA_{0.98}MLA_{0.02}PbI_3$ and 236 nm for $MA_{0.95}MLA_{0.05}PbI_3$ perovskite. Figure 3 shows the atomic force microscopy (AFM) images of annealed $MA_{1-x}MLA_xPbI_3$ (x= 0, 0.01, 0.02, 0.05) hetero structured perovskite films. The perovskite films exhibit smoother surface when increasing the MLAI content with R_q roughness value is 16.0 for $MAPbI_3$, 11.3 for $MA_{0.99}MLA_{0.01}PbI_3$, 8.9 for $MA_{0.98}MLA_{0.02}PbI_3$ and 5.7 for $MA_{0.95}MLA_{0.05}PbI_3$ perovskite. It is expected that these smooth morphology would improve the interfacial charge injection and thus improve the performance of the PSCs.

The UV-vis absorption spectra of $MA_{1-x}MLA_xPbI_3$ (x= 0, 0.01, 0.02, 0.05) hetero structured perovskite films is shown in Figure 4a. The large change was not observed in the spectra when the x of MLAI was varied from 0 to 0.05. The highest absorbance was achieved by $MA_{0.98}MLA_{0.02}PbI_3$ perovskite film, which can be attributed to the enhanced surface coverage of perovskite layer. Band gaps (Eg) of the $MA_{1-x}MLA_xPbI_3$ (x= 0, 0.01, 0.02, 0.05) hetero perovskites were estimated from Tauc plot (Figure S2). The Eg slightly shifted from 1.57 eV for pristine $MAPbI_3$ perovskite to 1.59 eV for $MA_{0.95}MLA_{0.05}PbI_3$ hetero structured perovskite. Valence band edges of the perovskite materials also changed slightly after incorporation of MLAI into the $MAPbI_3$ perovskite structure as determined from photoelectron spectroscopy in air, shown in Figure 4b. The valence band edges

shifted from -5.50 eV for $MAPbI_3$ to more negative values of -5.53 eV,-5.55eV and -5.58 eV, respectively. This result is similar with previous reports for 2D/3D perovskite materials.[17] Figure 4c and 4d show the photoluminescence (PL) and time-resolved photoluminescence (TRPL) curves for the $MA_{1-x}MLA_xPbI_3$ (x= 0, 0.01, 0.02, 0.05) hetero perovskite films. All the perovskite films were prepared on glass substrates to avoid the influence of charge injection among the absorber layer and electron transfer layer. the PL intensity of the perovskite films increased from x=0.01 to x=0.02, then decreased for x=0.05, where $MA_{0.98}MLA_{0.02}PbI_3$ perovskite showed the strongest PL peak. The PL intensity enhancement implies that incorporation of MLAI in the perovskite can reduce the presence of traps or defects and this will eventually reduce the recombination reaction. The TRPL curves was fitted by biexponetial curve fitting, given as equation (1), where τ_1 and τ_2 are best-fit PL decay times, A1 and A2 are the relative amplitudes. [18] The average effective lifetime (τ_{ave}) was estimated by equation (2).[19] The relative parameters of PL lifetime are summarized in Table S1. The τ_{ave} increases from 381 ns for $MAPbI_3$ to 491 ns for $MA_{0.99}MLA_{0.01}PbI_3$, and to the maximum of 570 ns for $MA_{0.98}MLA_{0.02}PbI_3$. This can be attributed to the improved surface morphology of the perovskite film. However, in the case of $MA_{0.95}MLA_{0.05}PbI_3$, the film shows decreased grain size which led to the decreased τ_{ave}(329 ns). These results indicate that proper MLAI incorporation can reduce the defect density in the perovskite film and thus reduce the recombination within the perovskite.

The effect of $MA_{1-x}MLA_xPbI_3$ (x= 0, 0.01, 0.02, 0.05) perovskite on the photovoltaic performance was investigated via planar FTO/SnO_2/Perovskite/P3HT/Spiro/Au perovskite solar cells. Figure 5a, 5b illustrate the schematic structure and energy diagram of the PSCs. The energy diagram of $MA_{1-x}MLA_xPbI_3$ (x= 0, 0.01, 0.02, 0.05) perovskite was obtained from the UV-Vis and PYS

measurement. Figure 5c shows the density–voltage (J–V) curves for the champion performance PSCs based on $MA_{1-x}MLA_xPbI_3$ perovskite material. The detail photovotic parameters are summarized in Table 1. There is a incresing trend of V_{OC} of the PSCs with the increase of MLAI content in the $MAPbI_3$ perovskite, from 1.02 V for pristine $MAPbI_3$ to 1.03 V for $MA_{0.99}MLA_{0.01}PbI_3$, 1.07 V for $MA_{0.98}MLA_{0.02}PbI_3$, and 1.08 V for $MA_{0.95}MLA_{0.05}PbI_3$. The increased V_{OC} maybe owning to the increased bandgap and smoother perovskite layer. The J_{SC} of the perovskite device increased from 20.25 mA/cm^2 for pristine $MAPbI_3$ to 20.63 mA/cm^2 for $MA_{0.99}MLA_{0.01}PbI_3$, 20.85 mA/cm^2 for $MA_{0.98}MLA_{0.02}PbI_3$, and decreased to 19.74 mA/cm^2 for $MA_{0.95}MLA_{0.05}PbI_3$. The Jsc trend follows the same trend as photoluminescence intensity trend of the $MA_{1-x}MLA_xPbI_3$ (x= 0, 0.01, 0.02, 0.05) perovskite. As a result, the most efficient PSC was achieved by the $MA_{0.98}MLA_{0.02}PbI_3$ 2D/3D perovskite with the power convertion efficiency (PCE) of 17.2%, along with a fill factor of 76.1% which is 25% higher than the pristine $MAPbI_3$ perovskite (13.7%). The calculated J_{SC} obtained by integrating the IPCE curve of $MAPbI_3$ and $MA_{0.98}MLA_{0.02}PbI_3$ was shown in Figure 7d. The J_{SC} value was in agreement with the measured value from the J-V curve. Figure S5 shows J–V curves of $MA_{1-x}MLA_xPbI_3$ (x, 0, 0.01, 0.02, 0.05) perovskite under reverse and forward voltage scans. Incorporation of MLAI can effictively decreased the hysteresis of perovskite devices as it is negligible for $MA_{0.98}MLA_{0.02}PbI_3$ devices shown in Figure S5c. There are many reports analyzing the origin of hysteresis in PSCs such as charge trapping and de-trapping as a result of crystal defects, band bending between the different interfaces and ionic motions within perovskite. Park et al. have reported adding melamine hydroiodide can effectively decrease the hysteresis of perovskite devices as surface passivation of perovskite grains.[20] In our opinion, MALA has three amine groups that may provide hydrogen bonding to $[PbI_6]^{4-}$. As shown in Scheme 1 and Figure S1b, we suppose that some MALA through

bonding to $[PbI_6]^{4-}$ to affect the crystal lattice of the $MAPbI_3$ perovskite and others functioned as $MAPbI_3$ grains surface passivation. Such low hysteresis could be attributed to the uniform growth of the $MAPbI_3$ layer proved by the FE-SEM and AFM images which effectively reduced the presence of grain boundaries and thus charge transfer between grains is more efficient. Further, indoor environment stability of $MAPbI_3$ and $MA_{0.98}MLA_{0.02}PbI_3$ PSCs without sealing was investigated and the result of normalized J_{SC}, V_{OC}, FF, and PCE as a function of time is shown in Figure 6. The $MA_{0.98}MLA_{0.02}PbI_3$ -based device shows excellent stability in ambient air, where unencapsulated $MA_{0.98}MLA_{0.02}PbI_3$ -based device maintains 91% of its initial PCE after 560 h at 30% RH. However, the PCE of the control device decreased to 33% of its initial value due to reduction of J_{SC}, V_{OC}, and FF. From the above results, we can get the conclusion that the photoviotic performance and stability of the PSCs can be enhanced by functionalizing MLAI into the $MAPbI_3$ perovskite.

Conclusion

In summary, we have demonstrated that melamine hydroiodide (MLAI) can be successfully embedded into $MAPbI_3$ perovskite lattice structure forming $MA_{1-x}MLA_xPbI_3$ hetero structured perovskite. Even at 25 mol% of MLAI content, no new phase formed in the perovskite structure which is a key point to retain the photovoltaic behavior of the perovskite solar cells. $MA_{0.98}MLA_{0.02}PbI_3$ 2D/3D structured perovskite showed higher UV-vis absorbance, stronger photoluminescence intensity, longer photoluminescence decay time and more denser morphology than the pristine $MAPbI_3$ perovskite which led to the power conversion efficiency (PCE) of 17.2% about 25% higher than the pristine $MAPbI_3$ perovskite (13.7%). Indoor environment stability test shows the superior stability performance of the $MA_{0.98}MLA_{0.02}PbI_3$ based devices, retaining over 91% of its original performance after 560 h without encapsulation. This work offers a new

approach to modify the ABX_3 perovskite materials with multi-amine organic material for enhancing the stability of perovskite without decreasing the photoviotic of the solar cell devices.

Supporting Information

Supporting Information is available from the Wiley Online Library or from the author.

Acknowledgements
((Acknowledgements, general annotations, funding. Other references to the title/authors can also appear here, such as "Author 1 and Author 2 contributed equally to this work."))

Received: ((will be filled in by the editorial staff))
Revised: ((will be filled in by the editorial staff))
Published online: ((will be filled in by the editorial staff))

References

[1] H.-S. Kim, C.-R. Lee, J.-H. Im, K.-B. Lee, T. Moehl, A. Marchioro, S.-J. Moon, R. Humphry-Baker, J.-H. Yum, J. E. Moser, M. Grätzel, N.-G. Park, *Scientific Reports* **2012**, 2, 591.

[2] a) N. J. Jeon, H. Na, E. H. Jung, T.-Y. Yang, Y. G. Lee, G. Kim, H.-W. Shin, S. Il Seok, J. Lee, J. Seo, Nature Energy **2018**, 3, 682; b) A. Kojima, K. Teshima, Y. Shirai, T. Miyasaka, Journal of the American Chemical Society **2009**, 131, 6050; c) W. S. Yang, B.-W. Park, E. H. Jung, N. J. Jeon, Y. C. Kim, D. U. Lee, S. S. Shin, J. Seo, E. K. Kim, J. H. Noh, Science **2017**, 356, 1376.

[3] H.-S. Kim, I.-H. Jang, N. Ahn, M. Choi, A. Guerrero, J. Bisquert, N.-G. Park, The journal of physical chemistry letters **2015**, 6, 4633.

[4] a) B. J. Kim, D. H. Kim, Y.-Y. Lee, H.-W. Shin, G. S. Han, J. S. Hong, K. Mahmood, T. K. Ahn, Y.-C. Joo, K. S. Hong, Energy & Environmental Science **2015**, 8, 916; b) S. N. Habisreutinger, T. Leijtens, G. E. Eperon, S. D. Stranks, R. J. Nicholas, H. J. Snaith, Nano letters **2014**, 14, 5561.

[5] T. Leijtens, G. E. Eperon, N. K. Noel, S. N. Habisreutinger, A. Petrozza, H. J. Snaith, Advanced Energy Materials **2015**, 5, 1500963.

[6] a) F. Yang, G. Kapil, P. Zhang, Z. Hu, M. A. Kamarudin, T. Ma, S. Hayase, ACS Applied Materials & Interfaces **2018**, 10, 16482; b) Y. Fu, K. M. Akmal, Z. Putao, K. Gaurav, M. Tingli, H. Shuzi, ChemSusChem **2018**, 11, 2348; c) N. J. Jeon, J. H. Noh, Y. C. Kim, W. S. Yang, S. Ryu, S. I. Seok, Nature materials **2014**, 13, 897; d) M. Konstantakou, D. Perganti, P. Falaras, T. Stergiopoulos, Crystals **2017**, 7, 291.

[7] a) F. Yang, M. A. Kamarudin, G. Kapil, D. Hirotani, P. Zhang, C. H. Ng, T. Ma, S. Hayase, ACS Applied Materials & Interfaces **2018**, 10, 24543; b) R. G. Niemann, L. Gouda, J. Hu, S. Tirosh, R. Gottesman, P. J. Cameron, A. Zaban, Journal of Materials Chemistry A **2016**, 4, 17819; c) J. Jin, H. Li, C. Chen, B. Zhang, L. Xu, B. Dong, H. Song, Q. Dai, ACS applied materials & interfaces **2017**, 9, 42875.

[8] a) P. Zhang, F. Yang, G. Kapil, Q. Shen, T. Toyoda, K. Yoshino, T. Minemoto, S. S. Pandey, T. Ma, S. Hayase, Organic Electronics **2018**, DOI: https://doi.org/10.1016/j.orgel.2018.06.038; b) D. Bi, C. Yi, J. Luo, J.-D. Décoppet, F. Zhang, S. M. Zakeeruddin, X. Li, A. Hagfeldt, M. Grätzel, Nature Energy **2016**, 1, 16142; c) F. Yang, H. E. Lim, F. Wang, M. Ozaki, A. Shimazaki, J. Liu, N. B. Mohamed, K. Shinokita, Y. Miyauchi, A. Wakamiya, Advanced Materials Interfaces **2018**, 5, 1701256; d) S. Kundu, T. L. Kelly, Materials Chemistry Frontiers **2018**, 2, 81. e) P. Zhang, F. Yang, M. A. Kamarudin, C. H. Ng, G. Kapil, T. Ma, S. Hayase, *ACS Applied Materials & Interfaces* **2018**, 10, 29630.

[9] a) Y. Chen, Y. Sun, J. Peng, J. Tang, K. Zheng, Z. Liang, Advanced Materials 2018, 30, 1703487; b) R. K Misra, B.-E. Cohen, L. Iagher, L. Etgar, ChemSusChem **2017**; c) J. Qing, X. K. Liu, M. Li, F. Liu, Z. Yuan, E. Tiukalova, Z. Yan, M. Duchamp, S. Chen, Y. Wang,

Advanced Energy Materials **2018**, 1800185. d) F. Yang, P. Zhang, M. A. Kamarudin, G. Kapil, T. Ma, S. Hayase, Advanced Functional Materials **2018,** 0, 1804856.

[10] a) F. Wang, W. Geng, Y. Zhou, H. H. Fang, C. J. Tong, M. A. Loi, L. M. Liu, N. Zhao, Advanced Materials **2016**, 28, 9986; b) B. Saparov, D. B. Mitzi, Chemical reviews **2016**, 116, 4558; c) H. Tsai, W. Nie, J.-C. Blancon, C. C. Stoumpos, R. Asadpour, B. Harutyunyan, A. J. Neukirch, R. Verduzco, J. J. Crochet, S. Tretiak, Nature **2016**, 536, 312.

[11] M. E. Kamminga, H.-H. Fang, M. R. Filip, F. Giustino, J. Baas, G. R. Blake, M. A. Loi, T. T. Palstra, Chemistry of Materials **2016**, 28, 4554.

[12] J. Lu, L. Jiang, W. Li, F. Li, N. K. Pai, A. D. Scully, C. M. Tsai, U. Bach, A. N. Simonov, Y. B. Cheng, Advanced Energy Materials **2017**, 7, 1700444.

[13] a) F. Yang, G. Kapil, P. Zhang, Z. Hu, M. A. Kamarudin, T. Ma, S. Hayase, ACS applied materials & interfaces **2018**, 10, 16482; b) Q. Chen, H. Zhou, Z. Hong, S. Luo, H.-S. Duan, H.-H. Wang, Y. Liu, G. Li, Y. Yang, Journal of the American Chemical Society **2013**, 136, 622; c) Y. Fu, K. M. Akmal, Z. PuTao, K. Gaurav, M. Tingli, H. Shuzi, ChemSusChem 0.

[14] a) J. Burschka, N. Pellet, S.-J. Moon, R. Humphry-Baker, P. Gao, M. K. Nazeeruddin, M. Grätzel, Nature **2013**, 499, 316; b) S. Sun, T. Salim, N. Mathews, M. Duchamp, C. Boothroyd, G. Xing, T. C. Sum, Y. M. Lam, Energy & Environmental Science 2014, 7, 399.

[15] J. Zhao, Y. Deng, H. Wei, X. Zheng, Z. Yu, Y. Shao, J. E. Shield, J. Huang, Science Advances **2017**, 3.

[16] W. Qiu, T. Merckx, M. Jaysankar, C. M. de la Huerta, L. Rakocevic, W. Zhang, U. Paetzold, R. Gehlhaar, L. Froyen, J. Poortmans, Energy & Environmental Science **2016**, 9, 484.

[17] a) P. Chen, Y. Bai, S. Wang, M. Lyu, J. H. Yun, L. Wang, Advanced Functional Materials **2018**, 28, 1706923; b) Z. Wang, Q. Lin, F. P. Chmiel, N. Sakai, L. M. Herz, H. J. Snaith, Nature **2017**, 2, 1.

[18] F. Yang, D. Hirotani, G. Kapil, M. A. Kamarudin, C. H. Ng, Y. Zhang, Q. Shen, S. Hayase, Angewandte Chemie International Edition **2018**, 57, 12745.

[19] J. Feng, Z. Yang, D. Yang, X. Ren, X. Zhu, Z. Jin, W. Zi, Q. Wei, S. F. Liu, Nano Energy **2017**, 36, 1.

[20] S.-G. Kim, J. Chen, J.-Y. Seo, D.-H. Kang, N.-G. Park, ACS Applied Materials & Interfaces **2018**, 10, 25372.

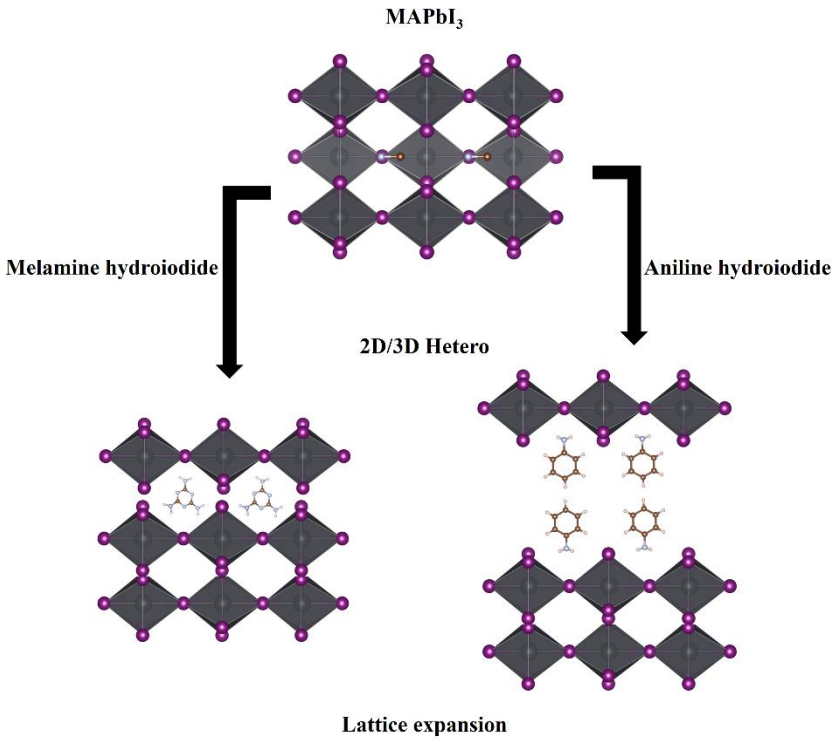

Scheme 1. Possible structural changes of $MA_{1-x}MLA_xPbI_3$ and 2D/3D hetero structured perovskite.

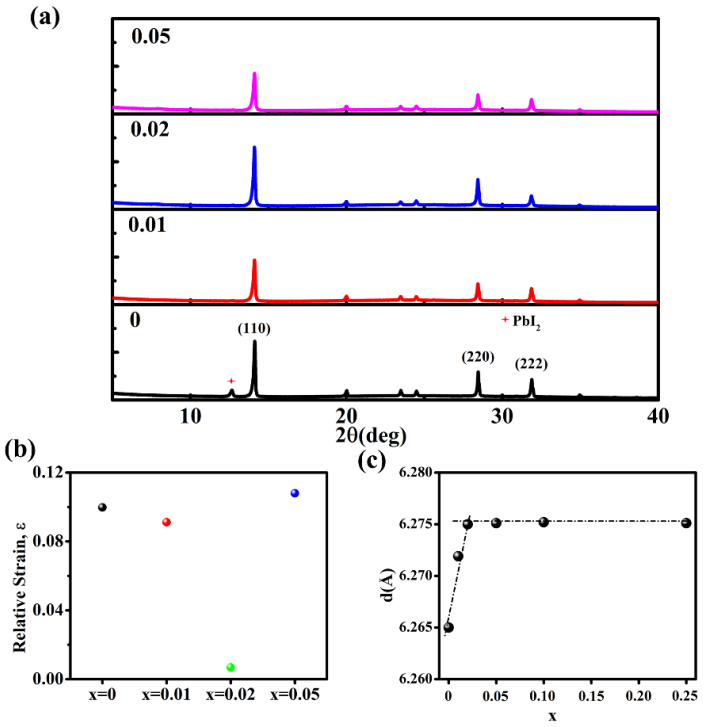

Figure 1. (a) X-ray diffraction, (b) Relative strain of $MA_{1-x}MLA_xPbI_3$ (x, 0, 0.01, 0.02, 0.05) films on glass substrates; (c) Interplanar (110) spacing as a function of different MLAI content.

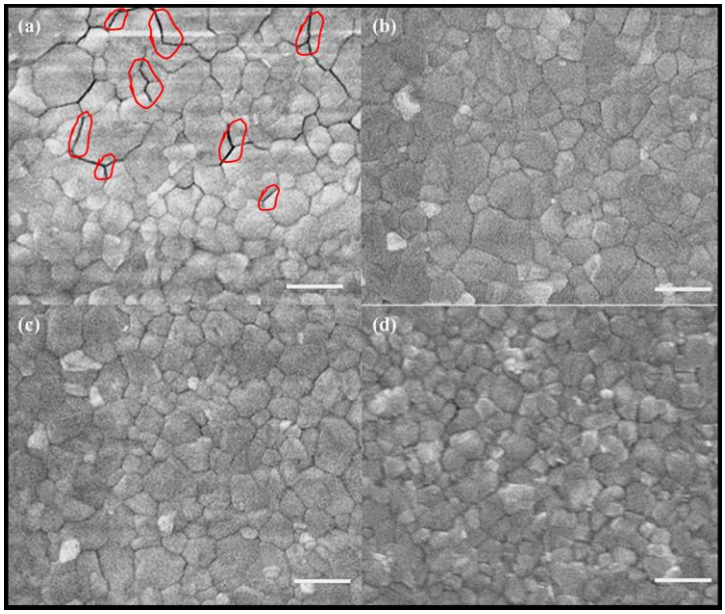

Figure 2. Top SEM images of the $MA_{1-x}MLA_xPbI_3$ (x, 0, 0.01, 0.02, 0.05) films on FTO glass substrates. (a) x=0; (b) x=0.01; (c) x=0.02; (d) x=0.05; The scale bar of the images is 500 nm.

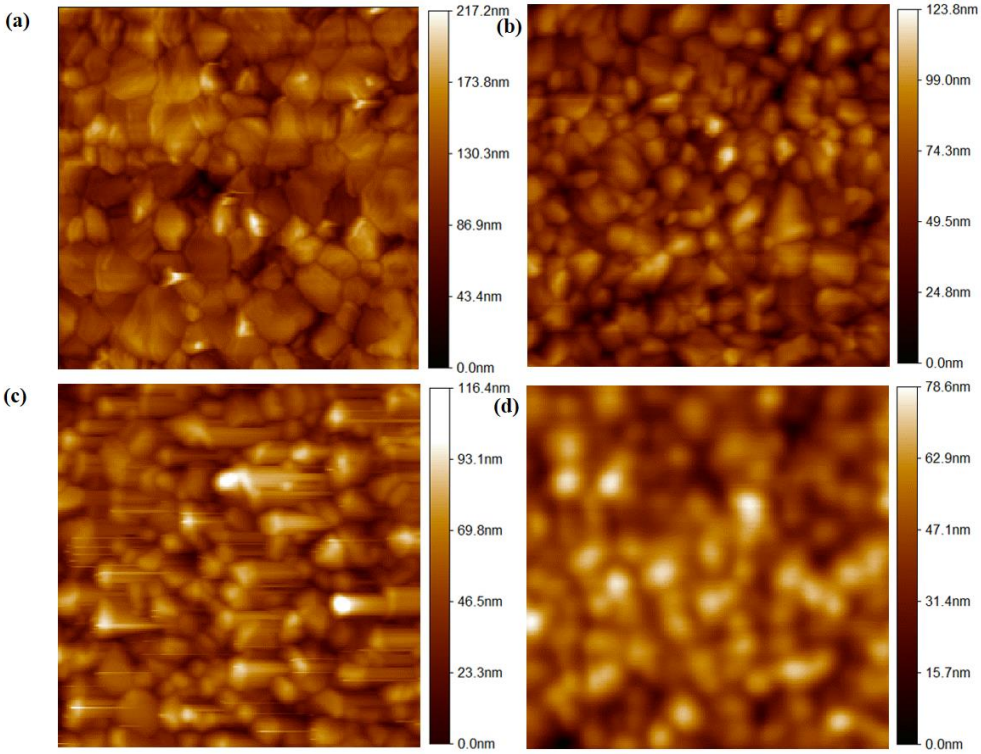

Figure 3. AFM height images of the $MA_{1-x}MLA_xPbI_3$ (x, 0, 0.01, 0.02, 0.05) films on glass substrates. (a) x=0; (b) x=0.01; (c) x=0.02; (d) x=0.05; The scanning dimension of the images is 4 μm × 4 μm.

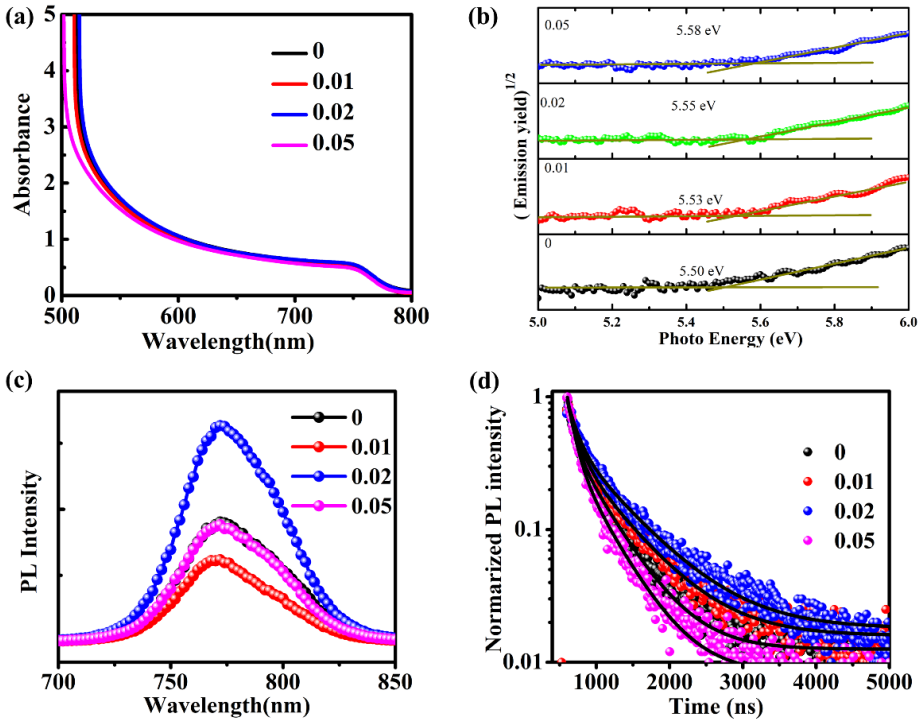

Figure 4. (a) UV-vis absorption of $MA_{1-x}MLA_xPbI_3$ (x, 0, 0.01, 0.02, 0.05) films on glass substrates; (b) PESA for $MA_{1-x}MLA_xPbI_3$ (x, 0, 0.01, 0.02, 0.05) films on FTO glass substrates; (c) PL and (d) TRPL spectra of $MA_{1-x}MLA_xPbI_3$ (x, 0, 0.01, 0.02, 0.05) films on glass substrates.

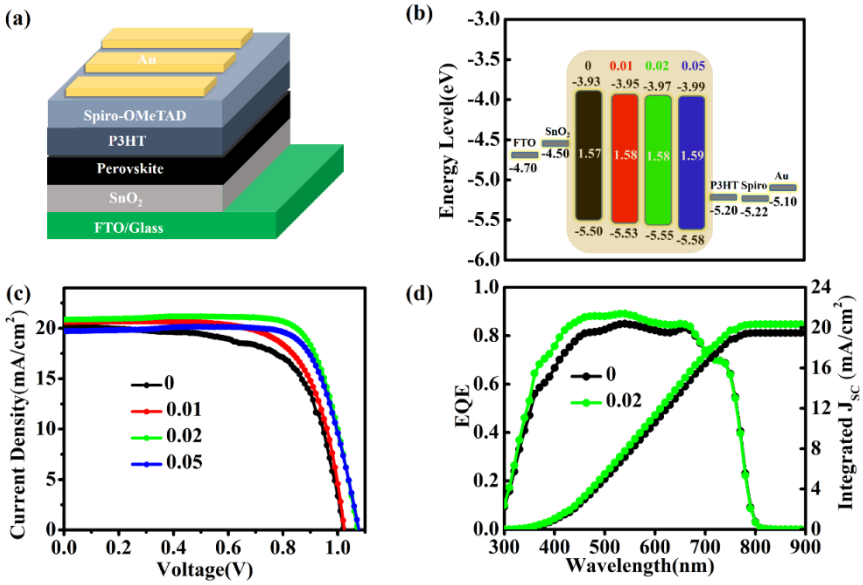

Figure 5. (a) Schematic diagram of FTO/SnO_2/perovskite/P3HT/Spiro-OMeTAD/Au planar perovskite solar cells. (b) Energy band diagram of the materials used in the planar perovskite solar cells. (c) J-V curves in reverse direction of $MA_{1-x}MLA_xPbI_3$ (x, 0, 0.01, 0.02, 0.05) planar perovskite solar cells. (d) EQE spectra of $MAPbI_3$ and $MA_{0.98}MLA_{0.02}PbI_3$ planar perovskite solar cells.

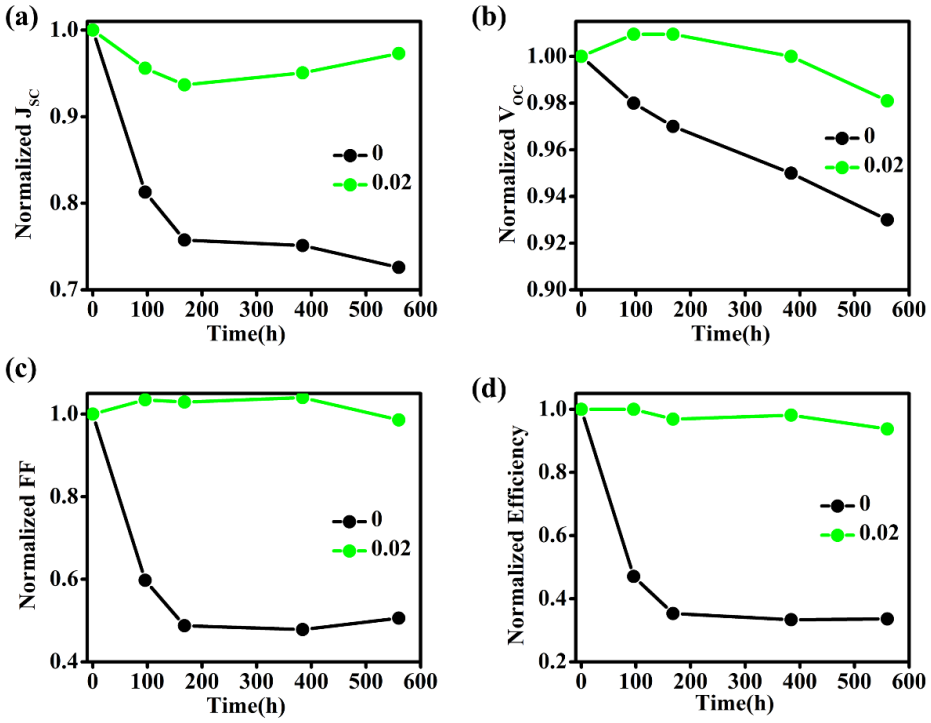

Figure 6. Stability test of $MAPbI_3$ and $MA_{0.98}MLA_{0.02}PbI_3$ planar perovskite solar cells without sealing in ambient atmosphere. (a) JSC; (b) VOC; (c) FF; (d) PCE.

Table 1. Photovoltaic parameters of champion $MA_{1-x}MLA_xPbI_3$ (x, 0, 0.01, 0.02, 0.05) perovskite solar cells.

x ratio	J_{sc} (mA/cm^2)	V_{OC} (V)	FF (%)	PCE (%)
0	20.25	1.02	66.4	13.7
0.01	20.63	1.03	69.6	14.7
0.02	20.85	1.07	77.1	17.2
0.05	19.74	1.08	75.7	16.2

$$A = A_0 + A_1 e^{-\frac{\tau-\tau 0}{\tau 1}} + A_2 e^{-\frac{\tau-\tau 0}{\tau 2}} \quad (1)$$

$$\tau_{ave} = \frac{\sum A_i \tau_i^2}{\sum A_i \tau_i} \quad (2)$$

Melamine hydroiodie (MLAI) has been successfully introduced for preparing the hetero structured $MAPbI_3$ perovskite for enhancing photovoltaic performance and stability of perovskite solar cells in robust humid ambient atmosphere (35 °C, 60-70% relative humidity). The power conversation efficiency of perovskite solar cells based on MLAI functionalized perovskite is 25% higher than that of pristine $MAPbI_3$ perovskite with nearly no hysteresis and high stability.

F. Yang, Dr. M. A. Kamarudin, D. Hirotani, P. T Zhang, Dr. G. Kapil, Dr. C. H. Ng, Prof. Dr. T. L. Ma, Prof. Dr. S. Hayase

Melamine Hydroiodide Functionalized $MAPbI_3$ Perovskite with Enhanced Photovoltaic Performance and Stability in Ambient Atmosphere

TOC figure ((Please choose one size: 55 mm broad ×50 mm high **or** 110 mm broad ×20 mm high. Please do not use any other dimensions))

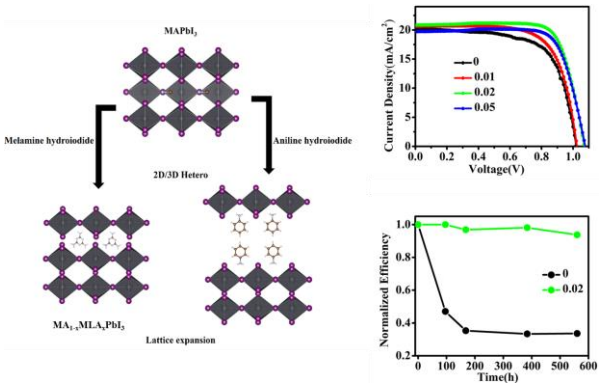

Experimental Section

Synthesis of **melamine hydroiodide (MLAI)**

MLAI was synthesized by reacting 2 g of melamine (Aldrich, 99%), 4 mL of hydroiodic acid (57 wt% in water with 1.5% hypophosphorous acid, Alfa Aesar), and 50 mL methanol in a 100 mL round bottom flask under nitrogen at 0 ^{o}C for 12 h with stirring. After reaction, the light white precipitate of MLAI filtered and washed with methanol, ethanol, and diethyl ether in sequence. Then compound MLAI was obtained as a slight white solid.

Preparation of perovskite solar cells

All reagents including ethyl acetate (Aldrich, 99.8 %) and chlorobenzene (Aldrich, 99.8%) were used without further purification. F-doped SnO_2 (FTO glass, Nippon Sheet Glass Co. Ltd) substrates were first patterned and cleaned using zinc powder and 6 N hydrochloric acid solution. Tin (II) chloride (Aldrich, 98 %) was dissolved in ethanol (Wako, 99.8 %) to form 0.1 M $SnCl_2$ solution. Then the $SnCl_2$ solution was spin-coated on the cleaned FTO glass in turn at 2000 rpm for 30 seconds and 6000rpm 30s. The substrate was annealed at 180 °C for 60 minutes on a hot plate to form a dense SnO_2 electron transport layer. The perovskite solution was prepared by dissolving 239 mg MAI (TCI, 98 %) and 692 mg PbI2 (TCI, 99.99 %) into 0.2 mL dimethyl sulfoxide (DMSO, Aldrich, 99.8 %) and 0.8 mL dimethylformamide (DMF, Aldrich, 99.8 %) to achieve 1.5 M MAPbI3 perovskite precursor solution. For preparing the 2D/3D perovskite precursor solution, keeping the PbI2 at 1.5M and adding a proper ELAI and MAI into 0.2 mL dimethyl sulfoxide (DMSO, Aldrich, 99.8 %) and 0.8 mL dimethylformamide. The perovskite layer was prepared on the FTO/SnO2 substrate by adding 0.1 mL perovskite precursor solution and spin-coated at 4000 rpm for 25 s. 0.5 mL ethyl acetate (99.8 %, Aldrich) antisolvent was dripped during the spin-coated progress. The spin-coated perovskite film was annealed at 100 °C for 10 min. Then 5mg/mL P3HT(TCI, 99%) chlorobenzene solution was spin-coating at 4000rpm for 25 seconds and anealled at 160 °C for 10 minutes. The Spiro-MeOTAD layer was then prepared by spin-coating a chlorobenzene solution containing 180 mM Spiro-MeOTAD (Aldrich, 99 %), 60 mM tert-butylpyridine (Aldrich, 96 %), 30 mM Li-TFSI (Aldrich, 99.95 %) (520 mg/mL in acetonitrile) and 33 mM FK209 (Aldrich, 99 %) (300 mg/mL in acetonitrile) at 4000 rpm for 30 seconds. Finally, 80 nm-thick Au counter electrode was deposited by thermal evaporation. All procedures were performed at around 35 ^{o}C, 60%-70% relative humidity in ambient air condition (Relative humidity was recorded using a hygrometer accurate to ± 5 % RH between 25 % and 69.9 % RH, ±10 % RH between 70 % and 90 % RH) (A&D Company, AD-5681)).

Characterization

Solar cell performance was measured by a solar simulator (CEP-2000SRR, Bunkoukeiki Inc., AM 1.5G 100 mWcm^{-2}) and a mask with exposure area 0.10 cm^2 was used during the photovoltaic measurements with a 0.1 V/s scanning rate in reverse (from the open-circuit voltage (V_{OC}) to the

short-current density (J_{SC})) and forward (from J_{SC} to V_{OC}) modes under standard global AM 1.5 illumination. The IPCE spectra were recorded using a monochromatic Xenon lamp (Bunkouki CEP-2000SRR). X-ray Diffraction (XRD) Study. The surface morphology of the samples was observed through a scanning electron microscope (SEM) (JEOL, Neoscope, JCM-6000). The XRD patterns were obtained by a Rigaku Smartlab X-ray diffractometer with monochromatic Cu-Kβ irradiation (45 kV/200 mA). The UV-Vis measurement was performed using a JASCO V-670. Spectrophotometer. E Photoelectron yield spectroscopy (PYS) was used to determine the valence band using a Bunkoukeiki KV205-HK ionization energy measurement system with – 5.0 V of applied voltage under 10^{-4} Pa vacuum.

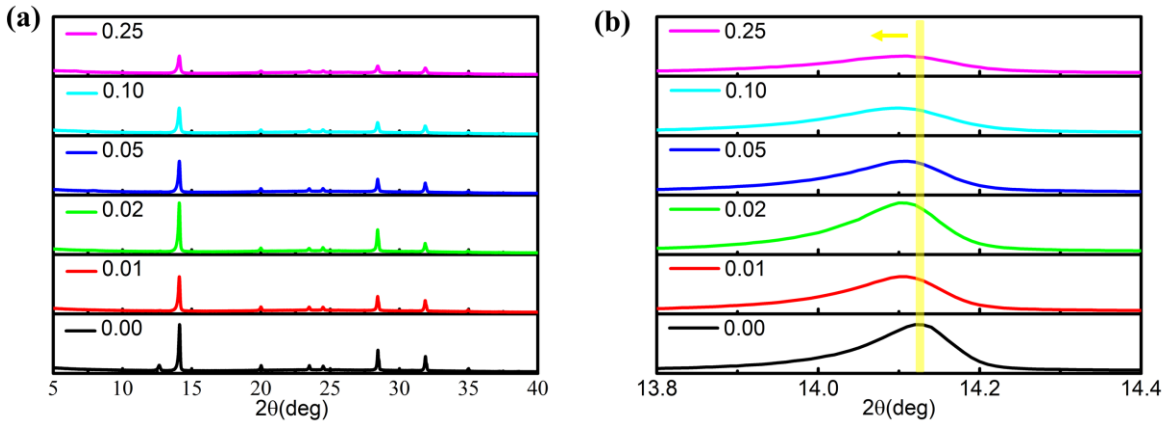

Figure S1 X-ray diffraction of $MA_{1-x}MLA_xPbI_3$ (x, 0, 0.01, 0.02, 0.05, 0.10, 0.25) films on glass substrates. (a) Wide range from 5º to 40º of 2θ; (b) Narrow range of the (110) diffraction. $(\alpha h\nu)^2$ versus light excitation energy hν.

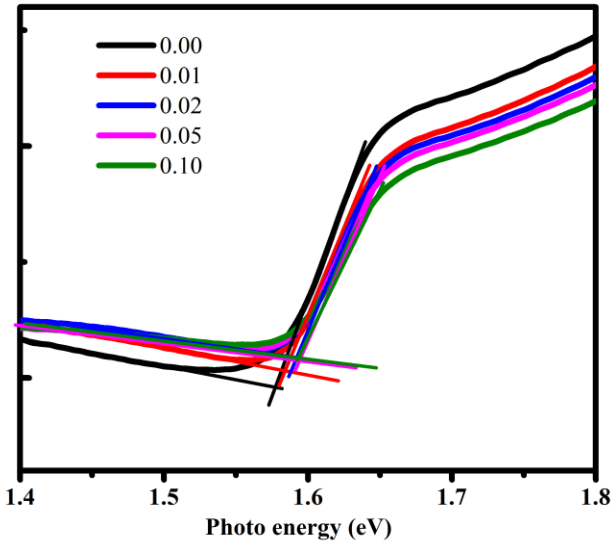

Figure S2 $(\alpha h\nu)^2$ versus light excitation energy hν of $MA_{1-x}MLA_xPbI_3$ (x, 0, 0.01, 0.02, 0.05, 0.10) perovskite materials.

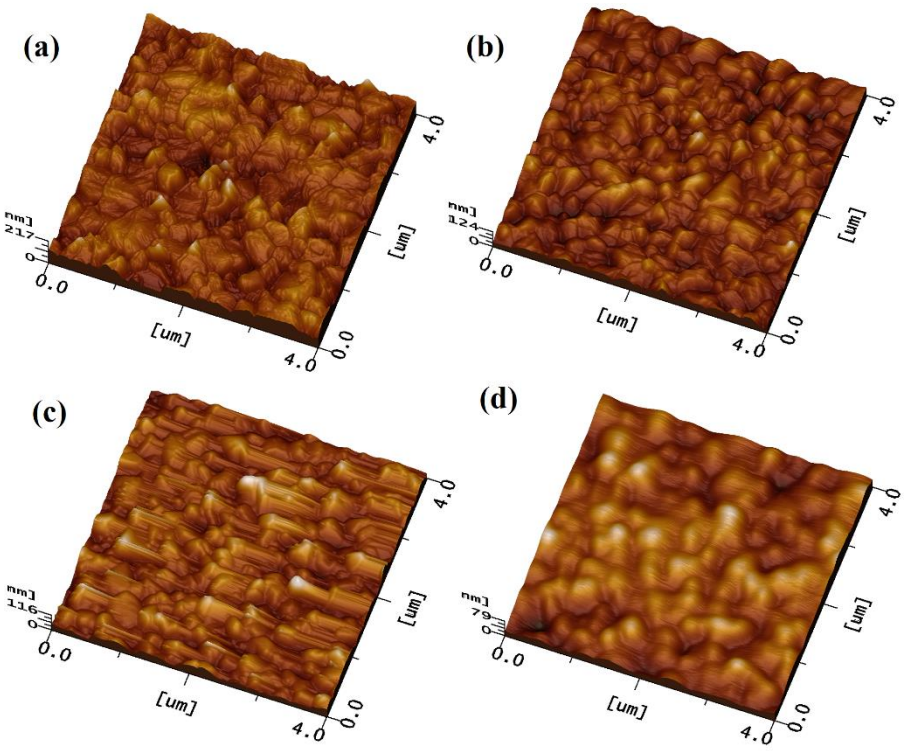

Figure S3. 3D surface plot images of $MA_{1-x}MLA_xPbI_3$ (x, 0, 0.01, 0.02, 0.05) perovskite materials. (a) x=0; (b) x=0.01; (c) x=0.02; (d) x=0.05.

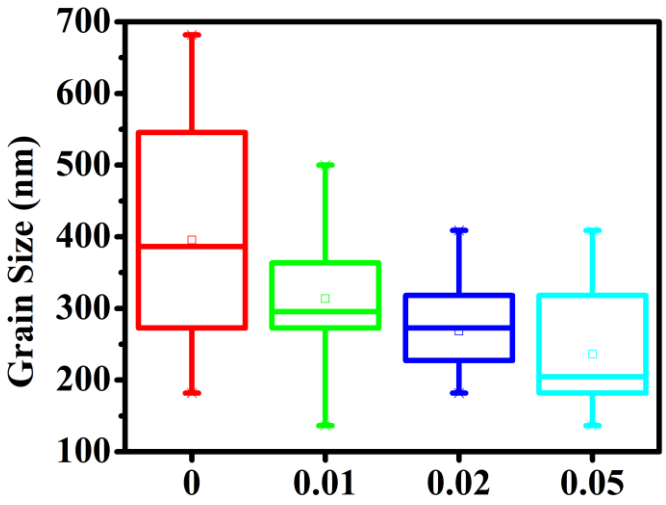

Figure S4. The statistical distribution of the particle size for $MA_{1-x}MLA_xPbI_3$ (x, 0, 0.01, 0.02, 0.05) perovskite films.

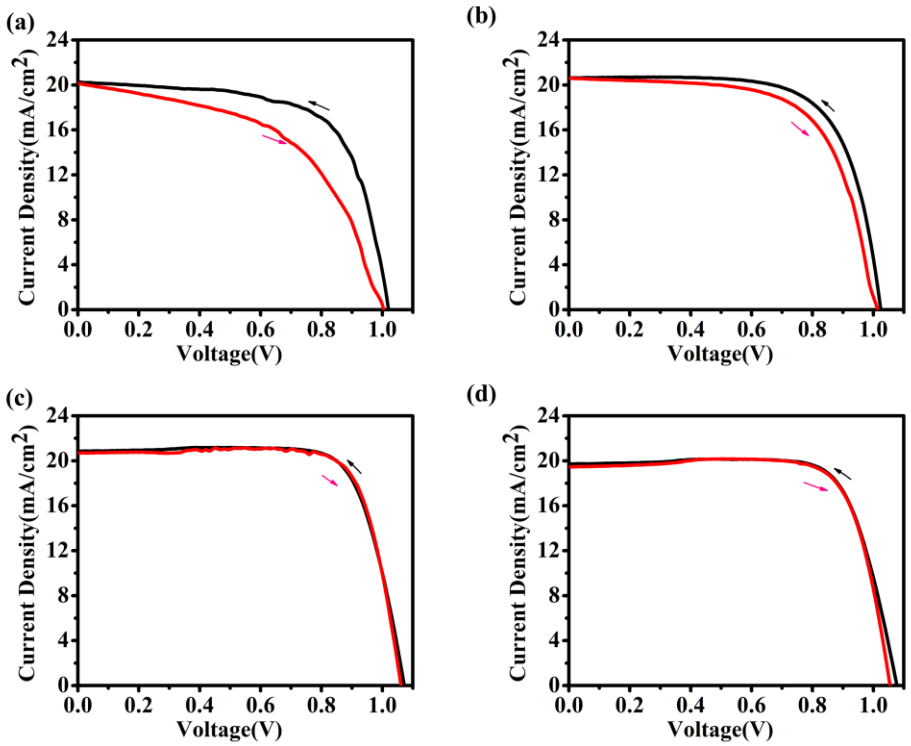

Figure S5. J−V curves of the champion planar PSCs based on $MA_{1-x}MLA_xPbI_3$ (x, 0, 0.01, 0.02, 0.05) perovskite under reverse and forward voltage scans. (a) x=0; (b) x=0.01; (c) x=0.02; (d) x=0.05.

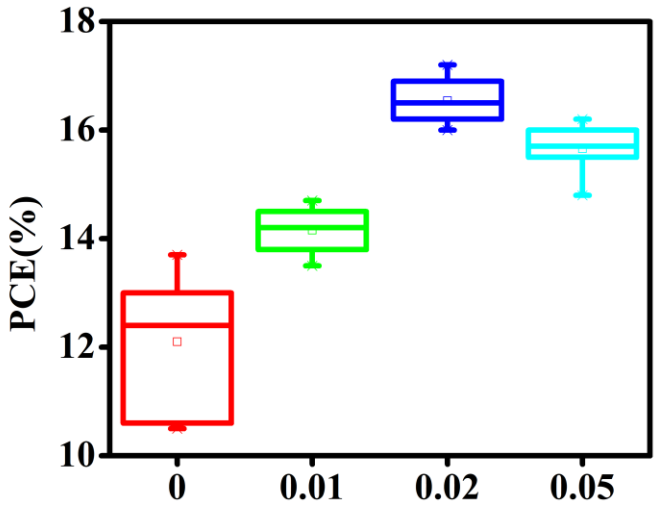

Figure S6. PCE statistics for the planar PSCs based on $MA_{1-x}MLA_xPbI_3$ (x, 0, 0.01, 0.02, 0.05) perovskite.

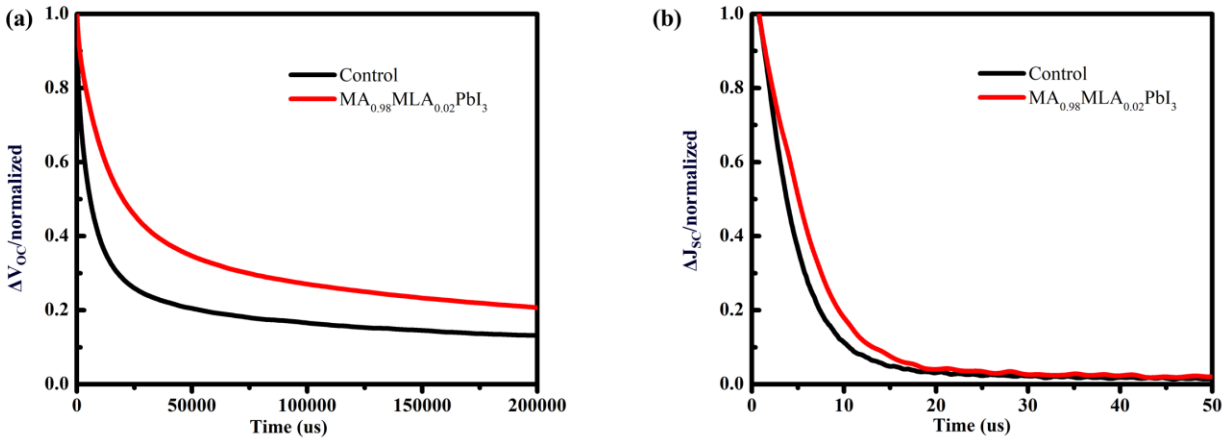

Figure S7. (a) Transient photovoltage decay curves of device $MAPbI_3$ and device $MA_{0.98}MLA_{0.02}PbI_3$ under open-circuit conditions. (b) Transient photocurrent decay curves of device $MAPbI_3$ and device $MA_{0.98}MLA_{0.02}PbI_3$ under short-circuit conditions.

x ratio	τ_1(ns)	A_1	τ_2 (ns)	A2	τ_{ave}(ns)
0	453	0.453	91	0.571	381
0.01	128	0.607	608	0.396	491
0.02	129	0.568	676	0.449	570
0.05	428	0.365	100	0.681	329

Table S1. Summary of the parameters fitted from the time-resolved PL spectra.